RSC Advances

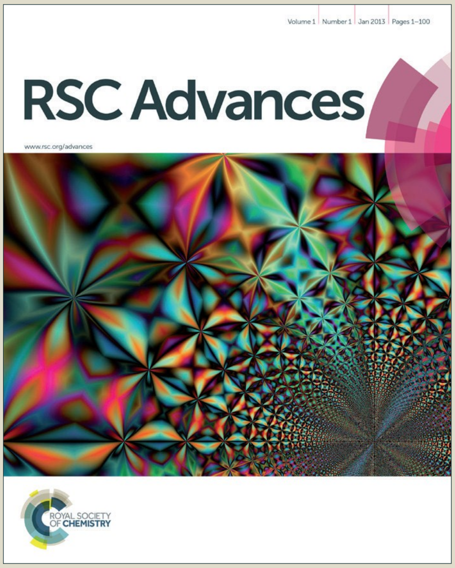

ROYAL SOCIETY OF CHEMISTRY

www.rsc.org/advances

Journal Name

ARTICLE

A new complex alkali metal aluminium amide borohydride, $Li_2Al(ND_2)_4BH_4$: synthesis, thermal analysis and crystal structure

Received 00th January 20xx,
Accepted 00th January 20xx

DOI: 10.1039/x0xx00000x

www.rsc.org/

S. Hino[a], T. Ichikawa[b], Y. Kojima[c], M. H. Sørby[a,*], B. C. Hauback[a]

The mixtures of alkali metal aluminium amide $MAl(ND_2)_4$ and alkali metal borohydride MBH_4 were synthesized using ball-milling. Thermal analysis and phase identifications of the $MAl(ND_2)_4$–MBH_4 system were performed by differential scanning calorimetry-thermogravimetric analysis, temperature programmed desorption-residual gas analysis, in-situ synchrotron radiation powder X-ray diffraction and Fourier transform Infrared spectroscopy. A previously unknown phase, $Li_2Al(ND_2)_4BH_4$, was formed in the samples of $LiAl(ND_2)_4$+2$LiBH_4$ and $NaAl(ND_2)_4$+2$LiBH_4$. Its crystal structure was solved and refined in the monoclinic space group $P2_1/c$, with a = 6.8582(3) Å, b = 11.3128(5) Å, c = 11.2117(4) Å, β = 124.186(5)°. $Li_2Al(ND_2)_4BH_4$ is the first reported compound containing both $[Al(ND_2)_4]^-$ and BH_4^- anions. The ball-milling of $NaAl(ND_2)_4$+2$NaBH_4$ and $KAl(ND_2)_4$+2KBH_4 gave mixtures of the starting materials. The synthesized samples desorbed ammonia in the temperature range between 50 and 200 °C and hydrogen above ~300 °C.

Introduction

Complex hydrides, e.g., metal alanates ($MAlH_4$), borohydrides (MBH_4) and amides (MNH_2), are ionic compounds of metal cations and covalently bonded complex anions (AlH_4^-, BH_4^-, NH_2^-). They have been studied as hydrogen storage materials possessing high gravimetric and volumetric hydrogen densities.[1] Researches have been focused on tailoring the properties of the system to have favourable kinetics and thermodynamics for hydrogen desorption and absorption at moderate temperature.[2, 3]

Lithium amide ($LiNH_2$) desorbs ammonia on thermal decomposition above ~300 °C, while the mixture with LiH desorbs hydrogen at lower temperature (>200 °C).[4] The dehydrogenated product is Li_2NH and higher temperature (>320 °C) is necessary for complete dehydrogenation into Li_3N.[5] The reversible hydrogen desorption/absorption reactions are described as follows:

$$LiNH_2 + 2LiH \leftrightarrow Li_2NH + LiH + H_2 \leftrightarrow Li_3N + 2H_2.$$

In the $LiNH_2$–$LiBH_4$ mixture it has been assumed that Li_3BN_2 is the hydrogen-free dehydrogenated state:[6, 7]

$$2LiNH_2 + LiBH_4 \rightarrow Li_3BN_2 + 4H_2.$$

As a result of the stabilization of the dehydrogenated state, less positive enthalpy (23 kJ/molH_2) for the dehydrogenation reaction would be required compared to pure $LiBH_4$ (75 kJ/molH_2) according to DFT calculations.[7] This results in release of ~10 wt% hydrogen at relatively low temperature around 250 °C.[6] It is also reported that an intermediate phase ($Li_4BN_3H_{10}$) is formed after ball milling of the mixture of $LiNH_2$ and $LiBH_4$.[8]

Metal aluminium amide ($MAl(NH_2)_4$), are compounds where H^- in metal alanate are substituted by NH_2^- ions. They desorbs ammonia at around 100 °C for M = Li, Na and K.[9, 10] In analogy to the $LiNH_2$–LiH system, the $LiAl(NH_2)_4$–LiH system has been studied. The ball-milled mixture of $LiAl(NH_2)_4$+4LiH desorbed >5.0 wt% of H_2 at 130 °C.[11] In the present study, the mixtures of alkali metal aluminium amides and borohydrides were prepared and thermal analysis and phase identification of the mixtures were performed.

Experimental

$LiBH_4$ (≥95%), $NaBH_4$ (≥99%) and KBH_4 (≥98%) were purchased from Sigma-Aldrich and $LiAl(ND_2)_4$, $NaAl(ND_2)_4$ and $KAl(ND_2)_4$ were synthesized as described elsewhere.[12] Mixtures of $LiAl(ND_2)_4$–$LiBH_4$ (denoted as S1), $NaAl(ND_2)_4$–$LiBH_4$ (S2), $NaAl(ND_2)_4$–$NaBH_4$ (S3) and $KAl(ND_2)_4$–KBH_4 (S4) in 1 : 2 molar ratios were ball-milled for 1 h (15 min milling + 15 min rest, 4 cycles) under 0.1 MPa Ar atmosphere using a Pulverisette 7 (Fritsch). The samples studied in this paper are shown in Table 1. Sample handling was carried out in a MBraun Unilab glovebox filled with purified Ar (<1 ppm O_2 and H_2O).

---

[a] *Physics Department, Institute for Energy Technology, P.O. Box 40, NO-2027 Kjeller, Norway.*
[b] *Graduate School of Integrated Arts and Sciences, Hiroshima University, 1-3-1 Kagamiyama, Higashi-Hiroshima, 739-8530, Japan.*
[c] *Institute for Advanced Materials Research, Hiroshima University, 1-3-1 Kagamiyama, Higashi-Hiroshima, 739-8530, Japan.*
[*] *Corresponding author. Tel.: +47 6380 6000; fax: +47 6381 0920. E-mail address: magnuss@ife.no (M. H. Sørby).*

† Electronic Supplementary Information (ESI) available: In-situ SR-PXD data for ball-milled samples of $LiAl(ND_2)_4$+2$LiBH_4$ and $NaAl(ND_2)_4$+2$LiBH_4$. See DOI: 10.1039/x0xx00000x

Table 1. The samples and their hydrogen contents.

Notation	Materials	Molar ratio	H content wt%[a]
S1	$LiAl(ND_2)_4$–$LiBH_4$	1 : 2	11.3
S2	$NaAl(ND_2)_4$–$LiBH_4$	1 : 2	10.1
S3	$NaAl(ND_2)_4$–$NaBH_4$	1 : 2	8.4
S4	$KAl(ND_2)_4$–KBH_4	1 : 2	6.7

[a] wt% in non-deuterated sample.

Powder X-ray diffraction (PXD) patterns were collected using Cu K_α radiation in a Bruker-AXS D8 Advance diffractometer equipped with a Göbel mirror and a LynxEye 1D strip detector. The samples were contained in rotating boron glass capillaries (0.8 mmϕ) filled and sealed under Ar atmosphere.

Fourier transform infrared (FTIR) spectrometer (ALPHA, Bruker) equipped with a 45° diamond attenuated total reflectance (ATR) accessory was used to collect IR spectra at room temperature (RT). The spectra were obtained in the range of 4000–400 cm^{-1} with a resolution of 2 cm^{-1} without any dilution of the samples.

Temperature programmed desorption (TPD) was performed under dynamic vacuum up to 500 °C using an in-house built setup. The samples were heated from RT to 500 °C with a ramp rate of 2 °C min^{-1}. The desorbed gas was analyzed with a MKS Microvision-IP residual gas analyzer (RGA).

Combined differential scanning calorimetry-thermogravimetric analysis (DSC-TGA) was carried out using a Netzsch STA 449 F3 Jupiter instrument with an Al sample crucible covered by a lid with a small hole. The samples were heated from RT to 500 °C with a ramp rate of 5 °C min^{-1} under a 50 mL min^{-1} Ar flow.

In situ synchrotron radiation (SR) PXD measurements (λ = 0.694118 Å) were carried out using a pixel area detector (Pilatus2M, DECTRIS) at the Swiss-Norwegian Beamlines (SNBL, BM01A) at the European Synchrotron Radiation Facility (ESRF), Grenoble, France. The samples were mounted in boron glass capillaries (0.5 mmϕ) fixed in a Swagelok fitting and kept under dynamic vacuum. A diffraction pattern was collected every 40 s (exposure time 30 s). The capillary was rotated 30° during exposure to improve the powder averaging. Measurements were carried out between RT and 500 °C with a ramp rate of 5 °C min^{-1}. The two-dimensional data were integrated to one-dimensional diffraction patterns using the Fit2D program.[13]

The Dicvol[14] and Chekcell[15] programs were used for unit cell and space group determination. The global optimization approach with parallel tempering as implemented in the FOX program[16, 17] was used for crystal structure determination. The structure refinements were carried out using the GSAS[18] software package with the EXPGUI[19] user interface based on the Rietveld method.[20, 21] The backgrounds were fitted by a 36-term Chebyshev polynomial. A pseudo-Voigt function[22] with asymmetry correction[23] was used to model the peak profile. Isotropic displacement parameters were refined with a common U_{iso} value for D- and H-atoms, respectively. The crystal structures were illustrated using the VESTA program.[24]

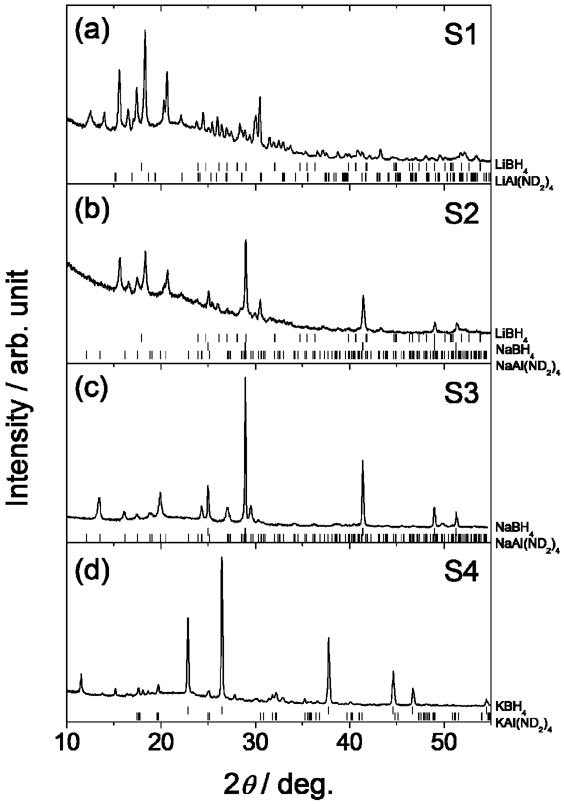

Figure 1. PXD patterns (Cu Kα) of ball-milled sample of (a) $LiAl(ND_2)_4$+2$LiBH_4$ (S1), (b) $NaAl(ND_2)_4$+2$LiBH_4$ (S2), (c) $NaAl(ND_2)_4$+2$NaBH_4$ (S3), and (d) $KAl(ND_2)_4$+2KBH_4 (S4). Bragg peak positions for the starting materials, as well as for $NaBH_4$ in S2, are marked with vertical ticks.

Results and discussion

Figure 1 shows PXD patterns of the samples after ball-milling. For sample S1, Bragg peaks from new phase(s) were observed, while no peaks remained from the starting materials. This indicates a complete chemical reaction. Similar for S2, the starting materials were not observed, and peaks from a new phase as well as $NaBH_4$ were found. The unidentified peaks in S2 are a subset of the unidentified peaks in the S1 sample. This indicates the possibilities that S1 contain the new phase observed in S2 in addition to other unidentified phase(s) or that the crystal structure of the phase in S1 has a superstructure of the one in S2. To our knowledge, the unidentified peaks from S1 and S2 do not match the reported structure of the Li-Al-B-N-H related compounds, such as $LiNH_2BH_3$,[25] $LiBH_4NH_3$,[26] $Li_4BH_4(NH_2)_3$,[8] $Li_2BH_4NH_2$,[27] $Al(BH_4)_3$,[28] $Al(NH_3)_6Li_2(BH_4)_5$,[29] $Al(BH_4)_3NH_3$[30] and $Al_3Li_4(BH_4)_{13}$.[31] For S3 only peaks from the starting materials were observed. For S4 the main peaks are also from the starting material, but in addition a small amount of a partially decomposed product[9] of $KAl(ND_2)_4$, i.e., $KAl(ND_2)_2ND$ is observed. This indicates that no chemical reaction occurred between the reactants during ball-milling.

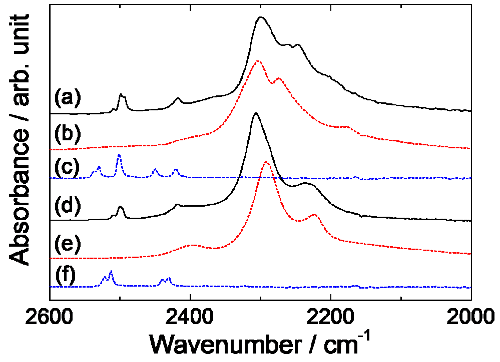

Figure 2. ATR-IR spectra of N-D and B-H stretching regions for: (a) $LiAl(ND_2)_4$+$2LiBH_4$ (S1), (b) $LiBH_4$, (c) $LiAl(ND_2)_4$, (d) $NaAl(ND_2)_4$+$2LiBH_4$ (S2), (e) $NaBH_4$, and (f) $NaAl(ND_2)_4$. All spectra were recorded under an Ar atmosphere at RT.

ATR-IR spectra of S1, S2 and the starting materials of each sample as references are shown in Figure 2. The peak positions are summarized in Table 2. Peaks corresponding to N-D and B-H stretching modes were observed in the IR spectra of both S1 and S2. Isotopic exchange between ND_2 and BH_4 groups was negligible since no peaks of N-H or B-D stretching mode were observed. The peak profile of B-H stretching mode in S1 was different from pure $LiBH_4$ (Figure 2b). Two main peaks were observed at 2303 and 2273 cm^{-1} in $LiBH_4$, while three peaks (2299, 2261 and 2247 cm^{-1}) were present in S1. Peaks corresponding to asymmetric stretching of ND_2 at 2537, 2530 and 2450 cm^{-1} in $LiAl(ND_2)_4$ (Figure 2c) were not apparent in S1 but the peaks at 2509 and 2426 (shoulder) might be due to ND2 stretching. Peak splitting (2499 and 2493 cm^{-1}) and slight red-shift were observed for symmetric stretching mode of ND_2 in S1. For sample S2, two main peaks in B-H region were observed at 2306 and 2236 cm^{-1}, respectively, and the most intense peak in $NaBH_4$ (2291 cm^{-1}) was present as a shoulder. Peaks corresponding to N-D stretching modes were almost the same as those in S1 and different from $NaAl(ND_2)_4$. Therefore, the unidentified phase(s) in S2 could contain both BH_4 and ND_2 ions. Here, we assume the composition of the phase to be $Li_2Al(ND_2)_4BH_4$. From the PXD-data (Figure 1), it is suggested that the following reaction occur during preparation of S2:

$$NaAl(ND_2)_4 + 2LiBH_4 \rightarrow Li_2Al(ND_2)_4BH_4 + NaBH_4$$

Gas desorption properties of the samples were investigated using TPD-RGA measurement (Figure 3). By analogy with $LiNH_2$–$LiBH_4$ and $LiAl(NH_2)_4$–LiH systems,[6,11] dominant release of hydrogen is expected, however, ND_3 (m/q = 20) was desorbed from all the samples above 50 °C. H_2 (m/q = 2) desorption was observed only above 250 °C in S1 and S2, 300 °C in S3 and 350 °C in S4. As described above from the IR data, H-D exchange between ND_2 and BH_4 groups was not apparent after ball-milling. HD (m/q = 3) would be released as a result of direct interaction of hydrogen atoms in the amide (ND_2^-) and borohydride (BH_4^-) ions. However, HD signals were synchronized with H_2 signals and less intense than H_2. This suggests that HD was generated from H_2 and D from ND_3 in the RGA chamber during ionization as a fragment of H_2 desorption. Small amounts of B_2H_6 (m/q = 27) were also released above 220 °C, 200 °C and 170 °C in S1, S2 and S3, respectively, while only a trace was detected from S4. The H_2 desorption temperature of S3 is much lower compared to the ball-milled $NaBH_4$ (>490 °C)[34] and similar to the $NaNH_2$-$NaBH_4$ system (>300 °C).[35] For MNH_2–MBH_4 it is proposed that an attraction between prontic $H^{\delta+}$ in NH_2 and hydridic $H^{\delta-}$ in BH_4 could accelerate the hydrogen desorption.[36] For the $MAl(ND_2)_4$–MBH_4 samples an attraction between $D^{\delta+}$ in ND_2 (or ND in metal aluminium imide $MAl(ND)_2$) and hydridic $H^{\delta-}$ in BH_4 could lower the hydrogen desorption temperature.

TGA-DSC profiles of the samples are shown in Figure 4. Two endothermic events at 60 and 100 °C without weight change were observed in S1, which might be due to phase transition(s). Ammonia desorption reactions appear as

Table 2. IR frequencies in cm^{-1} for N-D and B-H stretching modes and their assignments.

S1	$LiBH_4$	mode[†]	$LiAl(ND_2)_4$	mode[‡]	S2	$NaBH_4$	mode[†]	$NaAl(ND_2)_4$	mode[‡]
			2537	$\nu_aND_2(a)$					
2509			2530		2509			2522	ν_aND_2
2499			2501	$\nu_sND_2(a)$	2499			2512	
2493					2496				
2426sh			2450	$\nu_aND_2(b)$	2427sh			2438	ν_sND_2
2417			2420	$\nu_sND_2(b)$	2418			2430	
	2397	$\nu_2+\nu_4(A'')$/ $2\nu(A')$				2396	$\nu_2+\nu_4$		
2299	2303	$\nu_3(A')$			2306	2291	ν_3		
2261	2273								
2247									
	2177	$2\nu_4(A'')$			2236	2222	$2\nu_4$		

[†] From reference [32].

[‡] From reference [33]. The subscript a and s denotes asymmetric and symmetric vibration, respectively. The description (a) and (b) corresponds to two types of different ND_2 groups.

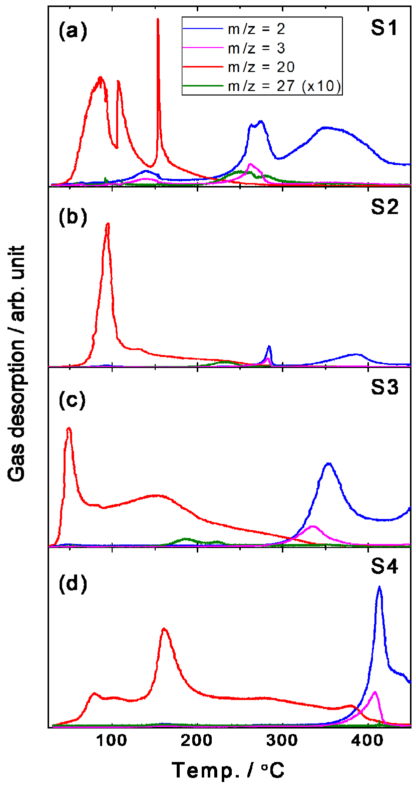

Figure 3. RGA results of the desorbed gas (m/z = 2 (H_2, blue), 3 (HD, magenta), 20 (ND_3, red), 27 (B_2H_6, green)) from the ball-milled samples (a) $LiAl(ND_2)_4$+2$LiBH_4$ (S1), (b) $NaAl(ND_2)_4$+2$LiBH_4$ (S2), (c) $NaAl(ND_2)_4$+2$NaBH_4$ (S3), and (d) $KAl(ND_2)_4$+2KBH_4 (S4). The heating rate was 2 °C/min. Intensity of B_2H_6 signals was multiplied by a factor of 10.

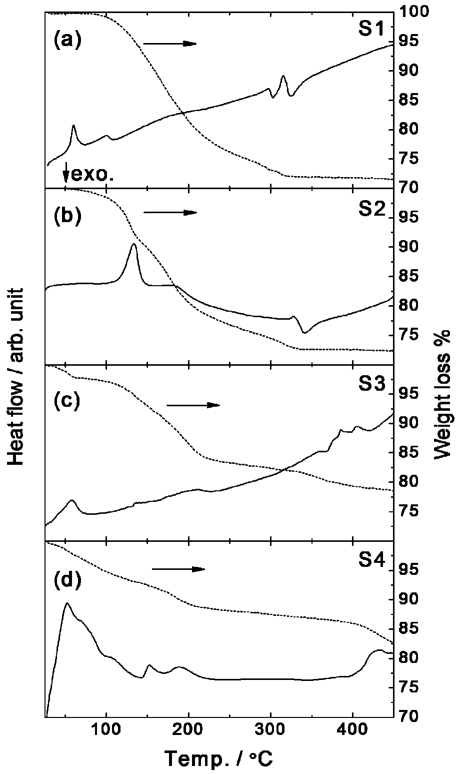

Figure 4. DSC (solid line) and TGA (dashed line) profiles of the ball-milled (a) $LiAl(ND_2)_4$+2$LiBH_4$ (S1), (b) $NaAl(ND_2)_4$+2$LiBH_4$ (S2), (c) $NaAl(ND_2)_4$+2$NaBH_4$ (S3), and (d) $KAl(ND_2)_4$+2KBH_4 (S4). The heating rate was 5 °C/min.

endothermic events in S2 (135 °C), S3 (60 °C) and S4 (150 °C). Weight losses below 250 °C were 23.8, 23.2, 16.7 and 11.8 wt% in the S1-S4 samples, respectively. The theoretical weight loss for 2 mole of ND_3 release which corresponds to decomposition of metal aluminium amides into metal aluminium imides ($MAl(NH)_2$) are 26.8, 24.2, 20.2 and 16.2 wt% in S1-S4, respectively. Considering the low decomposition temperatures of $NaAl(NH_2)_4$ and $KAl(NH_2)_4$, part of the aluminium amides would be decomposed during ball-milling in S3 and S4. Actually, PXD data shows the formation of the partially decomposed product in S4. Moreover, the end points of ammonia desorption are not very well defined, and some desorption continues also above 250°C. The total mass losses up to 450°C, which include hydrogen desorption, are 28.5, 27.7, 21.4 and 17.4 wt% for S1-S4, respectively. These are close to values for desorption of 2H_2 in addition to 2 ND_3, which are 29.5, 26.6, 22.3 and 17.9 wt%. This thus matches hydrogen desorption from the BH_4 unit in $Li_2Al(ND_2)_4BH_4$ in S1 and S2. It also indicate that a similar type of reaction takes place at elevated temperature in S3 and S4, since unreacted $NaBH4$ and KBH4 should not emit hydrogen in the investigated temperature range. The inconsistency of the temperatures for ammonia desorption between TGA-DSC and RGA resulted from different experimental conditions in these measurements. While the samples were under dynamic vacuum in the RGA measurements, an Al sample container was covered by a lid with a small hole in the TGA-DSC measurements. Thus, for TGA-DSC the decomposition can be suppressed by ammonia partial pressure around the sample. Moreover, faster heating rate was used in the TGA-DSC experiments (5 °C/min) than in RGA (2 °C/min).

Selected diffraction patterns of *in-situ* SR-PXD data for the S1 sample are shown in Figure 5 (The rest of the *in-situ* SR-PXD data for S1 and S2 are given as Electronic Supplementary Information). The peaks that were not observed in S2 disappear around 50 °C on heating S1 under vacuum. The remaining peaks, thus corresponding to those observed from S2, were successfully indexed with a monoclinic unit cell, $P2_1/c$, a = 6.8582(3) Å, b = 11.3128(5) Å, c = 11.2117(4) Å, β = 124.186(5)° at 53 °C. Crystal structure determination and refinement was performed, confirming the suggested composition $Li_2Al(ND_2)_4BH_4$. For the structure refinement, ND_2 and BH_4 units were treated as rigid bodies and the positions of

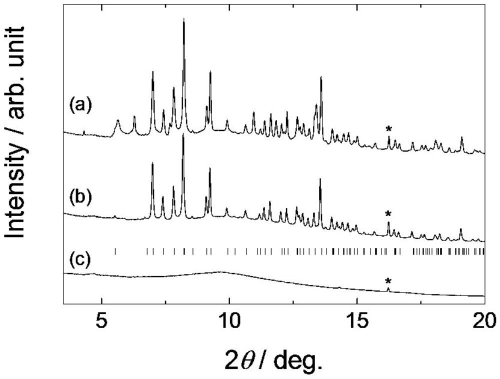

Figure 5. Selected *in-situ* SR-PXD patterns of LiAl$(ND_2)_4$+2LiBH$_4$ (S1) at (a) RT, (b) 53 °C and (c) 80 °C with λ = 0.694118 Å. "*" denotes diffraction peak from Li. Bragg peak positions for the monoclinic phase Li$_2$NaAl$(ND_2)_4$BH$_4$ are marked with vertical ticks.

hydrogen atoms are uncertain. N-D and B-H distances of 1.01 and 1.25 Å, D-N-D and H-B-H angles of 98.19 and 109.47°, respectively, were applied for the rigid bodies. The fit obtained in the Rietveld refinement based on the *in-situ* SR-PXD data at 53 °C for S1 is shown in Figure 6. Table 3 summarizes the structural parameters of Li$_2$Al$(ND_2)_4$BH$_4$ and the structure model is visualized in Figure 7. Al is tetrahedrally coordinated by ND$_2$ groups and the average Al-N distance is 1.974 Å which is slightly longer than that in LiAl$(ND_2)_4$ (1.868 Å).[12] The average Li-N distance (2.16 Å) of Li$_2$Al$(ND_2)_4$BH$_4$ is almost the same as that of LiAl$(ND_2)_4$ (2.100 Å). In LiBH$_4$, BH$_4$ group is tetrahedrally coordinated by Li atoms (average Li-B distance, 2.515 Å),[37] while planar Li$_2$B$_2$ units are linked by corner sharing where each B is shared between 2 planar units in Li$_2$Al$(ND_2)_4$BH$_4$ (average Li-B distance, 2.63 Å), yielding a 4-coordination which is neither tetrahedral nor planar. The average distance between N in ND$_2$ group and B in BH$_4$ group is 3.955 Å, and ND$_2$ and BH$_4$ groups are well-separated (3.77 Å or more).

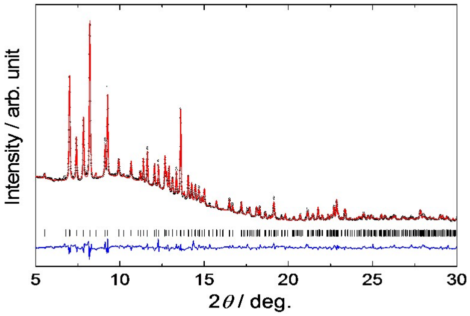

Figure 6. Rietveld refinement of the *in-situ* SR-PXD pattern of LiAl$(ND_2)_4$+2LiBH$_4$ (S1) at 53 °C with λ = 0.694118 Å. The region from 16.2 to 16.4° was excluded because of the reflection from Li phase. The black dot, red and blue lines are the observed, calculated and difference between observed and calculated patterns, respectively. Vertical tick marks show the position of the Bragg peaks.

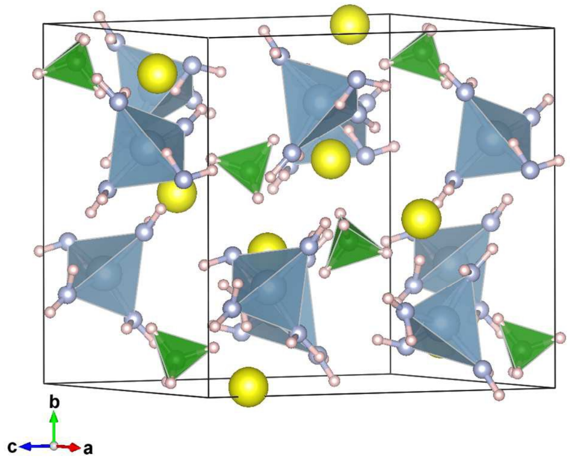

Figure 7. Visualization of the crystal structure of Li$_2$Al$(ND_2)_4$BH$_4$. Li: yellow spheres, Al: in centers of blue tetrahedra, N: gray spheres, B: in centers of green tetrahedra, H(D): pink spheres.

After heating up to ~80 °C in Figure 5c, the Bragg peaks of the monoclinic Li$_2$Al$(ND_2)_4$BH$_4$ disappeared as a result of amorphization and/or decomposition. It should be noted that metallic Li was observed in the PXD profile of S1 while it was found neither in the starting material LiAl$(ND_2)_4$ nor in S2. This indicates that metallic Li is formed in a redox process in conjunction with formation of the unknown phase which is only observed in S1.

Conclusions

Thermal and phase analyses of the MAl$(ND_2)_4$–MBH$_4$ systems were carried out by means of TGA-DSC, RGA, PXD and IR measurements. Ball-milled mixtures of LiAl$(ND_2)_4$+2LiBH$_4$ (S1), NaAl$(ND_2)_4$+2LiBH$_4$ (S2), NaAl$(ND_2)_4$+2NaBH$_4$ (S3) and KAl$(ND_2)_4$+2KBH$_4$ (S4) desorbed ammonia in the temperature range between 50 and 200 °C and hydrogen above ~300 °C. From the PXD results, mixture of the starting materials were found in the sample of NaAl$(ND_2)_4$+2NaBH$_4$ (S3) and KAl$(ND_2)_4$+2KBH$_4$ (S4), while previously undescribed phases were observed in the sample of LiAl$(ND_2)_4$+2LiBH$_4$ (S1) and NaAl$(ND_2)_4$+2LiBH$_4$ (S2). Structure determination of the novel phase Li$_2$Al$(ND_2)_4$BH$_4$, found in both S1 and S2, was performed and it is revealed that the phase has the monoclinic unit cell ($P2_1/c$) which contains $[Al(ND_2)_4]^-$ and BH_4^- anions.

Acknowledgements

The EU FP7 Marie Curie Action Incoming International Fellowship project MATERHY (FP7-PEOPLE-2009-IIF, no. 253863) is acknowledged for financial support. The authors acknowledge the skillful assistance from the staff of the Swiss-Norwegian Beamline, at the European Synchrotron Radiation Facility, Grenoble, France.

References

1 S. Orimo, Y. Nakamori, J. R. Eliseo, A. Zuettel, C. M. Jensen, *Chem Rev.*, 2007, **107**, 4111-4132.
2 J. Wang, H.-W. Li and P. Chen, *Mrs Bulletin*, 2013, **38**, 480-487.
3 L. H. Jepsen, M. B. Ley, Y.-S. Lee, Y. W. Cho, M. Dornheim, J. O. Jensen, Y. Filinchuk, J. E. Jorgensen, F. Besenbacher and T. R. Jensen, *Mater. Today*, 2014, **17**, 129-135.
4 T. Ichikawa, S. Isobe, N. Hanada and H. Fujii, *J. Alloys Compd.*, 2004, **365**, 271-276.
5 P. Chen, Z. T. Xiong, J. Z. Luo, J. Y. Lin and K. L. Tan, *Nature*, 2002, **420**, 302-304.
6 F. E. Pinkerton, G. P. Meisner, M. S. Meyer, M. P. Balogh and M. D. Kundrat, *J. Phys. Chem. B*, 2005, **109**, 6-8.
7 M. Aoki, K. Miwa, T. Noritake, G. Kitahara, Y. Nakamori, S. Orimo and S. Towata, *Appl. Phys. A-Mater.*, 2005, **80**, 1409-1412.
8 Y. E. Filinchuk, K. Yvon, G. P. Meisner, F. E. Pinkerton and M. P. Balogh, *Inorg. Chem.*, 2006, **45**, 1433-1435.
9 R. Brec and J. Rouxel, *Bull. Soc. Chim. Fr.*, 1968, 2721-2726.
10 T. Ono, K. Shimoda, M. Tsubota, S. Hino, K. Kojima, T. Ichikawa and Y. Kojima, *J. Alloys Compd.*, 2010, **506**, 297-301.
11 R. Janot, J. B. Eymery and J. M. Tarascon, *J. Phys. Chem. C*, 2007, **111**, 2335-2340.
12 S. Hino, H. Grove, T. Ichikawa, Y. Kojima, M. H. Sorby and B. C. Hauback, *Int. J. Hydrogen Energy, In press*. doi:10.1016/j.ijhydene.2015.05.012
13 A. P. Hammersley, *FIT2D: An Introduction and Overview*, 1997.
14 A. Boultif and D. Louer, *J. Appl. Crystallogr.*, 1991, **24**, 987-993.
15 B. L. Bochu, J, Suite of Programs for the Interpretation of X-ray Experiments, http://www.ccp14.ac.uk/tutorial/lmgp
16 V. Favre-Nicolin and R. Cerny, *J. Appl. Crystallogr.*, 2002, **35**, 734-743.
17 V. Favre-Nicolin and R. Cerny, *Z. Kristallogr.*, 2004, **219**, 847-856.
18 A. C. Larson and R. B. Von Dreele, *General Structure Analysis System (GSAS)*, 1994.
19 B. H. Toby, *J. Appl. Crystallogr.*, 2001, **34**, 210-213.
20 H. M. Rietveld, *Acta Crystallogr.*, 1967, **22**, 151-&.
21 H. M. Rietveld, *J. Appl. Crystallogr.*, 1969, **2**, 65-&.
22 P. Thompson, D. E. Cox and J. B. Hastings, *J. Appl. Crystallogr.*, 1987, **20**, 79-83.
23 L. W. Finger, D. E. Cox and A. P. Jephcoat, *J. Appl. Crystallogr.*, 1994, **27**, 892-900.
24 K. Momma and F. Izumi, *J. Appl. Crystallogr.*, 2011, **44**, 1272-1276.
25 H. Wu, W. Zhou and T. Yildirim, *J. Am. Chem. Soc.*, 2008, **130**, 14834-14839.
26 S. R. Johnson, W. I. F. David, D. M. Royse, M. Sommariva, C. Y. Tang, F. P. A. Fabbiani, M. O. Jones and P. P. Edwards, *Chem.-Asian. J.*, 2009, **4**, 849-854.
27 P. A. Chater, W. I. F. David and P. A. Anderson, *Chem. Commun.*, 2007, 4770-4772.
28 K. Miwa, N. Ohba, S. Towata, Y. Nakamori, A. Zuettel and S. Orimo, *J. Alloys Compd.*, 2007, **446**, 310-314.
29 Y. Guo, H. Wu, W. Zhou and X. Yu, *J. Am. Chem. Soc.*, 2011, **133**, 4690-4693.
30 É. B. Lobkovskii, V. B. Polyakova, S. P. Shilkin and K. N. Semenenko, *J. Struct. Chem.*, 1975, **16**, 66-72.
31 I. Lindemann, R. Domenech Ferrer, L. Dunsch, Y. Filinchuk, R. Cerny, H. Hagemann, V. D'Anna, L. M. L. Daku, L. Schultz and O. Gutfleisch, *Chem.-Eur. J.*, 2010, **16**, 8707-8712.
32 O. Zavorotynska, M. Corno, A. Damin, G. Spoto, P. Ugliengo and M. Baricco, *J. Phys. Chem. C*, 2011, **115**, 18890-18900.
33 R. Brec, A. Novak and J. Rouxel, *Bull. Soc. Chim. Fr.*, 1967, 2432-2435.
34 J. Mao, Z. Guo, X. Yu and H. Liu, *J. Phys. Chem. C*, 2011, **115**, 9283-9290.
35 P. A. Chater, P. A. Anderson, J. W. Prendergast, A. Walton, V. S. J. Mann, D. Book, W. I. F. David, S. R. Johnson and P. P. Edwards, *J. Alloys Compd.*, 2007, **446**, 350-354.
36 Y. Zhang and Q. F. Tian, *Int. J. Hydrogen Energy*, 2011, **36**, 9733-9742.
37 J. P. Soulié, G. Renaudin, R. Černý and K. Yvon, *J. Alloys Compd.*, 2002, **346**, 200-205.

Table 3. Results from SR-PXD Rietveld refinement of $Li_2Al(ND_2)_4BH_4$ (R_{wp} = 1.70%) at 53 °C. Estimated standard deviations are in parentheses.

Space group: $P2_1/c$ (No. 14), $Z = 4$, $T = 53$ °C

$a = 6.8582(3)$ Å, $b = 11.3128(5)$ Å, $c = 11.2117(4)$ Å, $\beta = 124.186(5)$°

Atom	Site	x	y	Z	U_{iso} / Å^2
Li1	4e	0.935(5)	0.477(2)	0.354(3)	0.10(1)
Al	4e	0.1187(8)	0.3074(4)	0.8821(4)	0.060(2)
N1	4e	0.0269(11)	0.1716(7)	0.7549(5)	0.024(3)
D1	4e	0.0314(11)	0.1063(7)	0.6951(5)	0.80(10)
D2	4e	0.1837(11)	0.1554(7)	0.8481(5)	0.80(10)
N2	4e	0.8126(14)	0.3829(5)	0.8405(7)	0.060(3)
D3	4e	0.8421(14)	0.3610(5)	0.9367(7)	0.80(10)
D4	4e	0.8913(14)	0.3125(5)	0.8290(7)	0.80(10)
N3	4e	0.3151(15)	0.2609(6)	0.0817(10)	0.064(4)
D5	4e	0.4121(15)	0.2181(6)	0.1770(10)	0.80(10)
D6	4e	0.4112(15)	0.3360(6)	0.1104(10)	0.80(10)
N4	4e	0.2822(13)	0.4280(6)	0.8437(7)	0.047(3)
D7	4e	0.3745(13)	0.4957(6)	0.8398(7)	0.80(10)
D8	4e	0.1236(13)	0.4469(6)	0.7530(7)	0.80(10)
B	4e	0.6969(17)	0.0906(7)	0.9505(8)	0.013(4)
H1	4e	0.5227(17)	0.0230(7)	0.8924(8)	0.10(2)
H2	4e	0.6572(17)	0.1782(7)	0.0018(8)	0.10(2)
H3	4e	0.7334(17)	0.1244(7)	0.8585(8)	0.10(2)
H4	4e	0.8743(17)	0.0369(7)	0.0492(8)	0.10(2)
Li2	4e	0.560(5)	0.124(2)	0.120(3)	0.15(1)

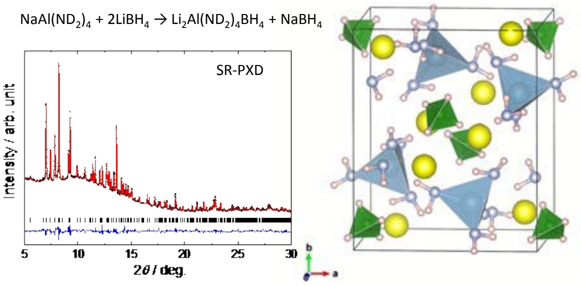

The first reported compound containing both $[Al(ND_2)_4]^-$ and BH_4^- anions, $Li_2Al(ND_2)_4BH_4$, was formed in ball-milled $LiAl(ND_2)_4$+2$LiBH_4$ and $NaAl(ND_2)_4$+2$LiBH_4$. Its crystal structure was solved and refined in a monoclinic unit cell.